A Modular Physically Based Approach to the Sound Synthesis of Membrane Percussion Instruments

Federico Avanzini and Riccardo Marogna

***Abstract*—This paper presents a set of novel physical models for sound synthesis of membrane percussion instruments. First, a model for tension modulation in a struck circular membrane is discussed, which simulates the dynamic variations of partial frequencies occurring at large amplitude vibrations of the membrane. It is shown that the model, which is derived from a more general theory of nonlinear elastic plates, can be efficiently integrated into a modal synthesis engine. Novel models for two relevant sound production mechanisms in membrane percussions are then proposed, i.e., coupling between two membranes through enclosed air in two-headed percussions, and string-membrane coupling. Both are based on a lumped modeling approach and can be straightforwardly connected to the nonlinear membrane model. By virtue of this modular approach, individual elements (circular linear/nonlinear membranes, impact force, membrane coupling through air, string-membrane coupling) can be combined to form different instruments. The acoustic results of the proposed models are demonstrated by means of analysis of numerical simulations.**

***Index Terms*—Membrane percussion instrument, modal synthesis, musical instruments, nonlinear systems, physical modeling.**

I. Introduction

PERCUSSIONS, and particularly membrane percussions, are amongst the most ancient musical instruments and have evolved in a myriad of species over the millennia. According to the musical acoustics literature [1] they can be classified into three broad categories: those composed of a single membrane (or head) coupled to an enclosed air cavity, those composed of a single membrane supported by an open shell, and those composed of two heads coupled through an enclosed air cavity (the "batter" head is struck by the player, the "carry" head resonates due to coupling). Moreover, other resonating and interacting elements are often present.

Playing styles also vary considerably: membranes may be struck with a wooden stick or a mallet or the bare hand, brushed, tuned with a tuning pedal, damped and loaded in a variety of ways. Moreover the fine characteristics of the materials affect the sound quality: heads can be clear or coated, single or two-ply layered, and shells made of different qualities of woods, or metals, or plastics, also contribute in different ways to instrumental timbre. However, especially the role of the shell material is not completely clarified by the limited amount of studies (and one may even argue that such role is not always as relevant as common belief by musicians would suggest, similarly to other instruments [2], [3]).

For all these reasons membrane percussions represent a challenge for sound synthesis. One of the most promising and rapidly advancing approaches to sound synthesis is physical modeling, i.e., algorithms that simulate the sound generating mechanisms in the system of interest. Possibly the main advantage over traditional methods reside in physically meaningful model parameters, which allow intuitive interaction with the models. Two recent tutorial papers [4], [5] discuss trends and future directions in physical modeling of musical instruments, and show that membrane percussions are relatively less studied than other classes of instruments, such as strings or winds.

Signal-based approaches to percussion sound synthesis, based on source-filter decompositions, have been proposed in the early 1990s [6], [7]. Cook [8] developed a series of "physically informed" approaches to the modeling of percussion sounds. Physically based approaches have been mainly based on 2-D or 3-D digital waveguide meshes (digital waveguide mesh (DWM) [9]). These computational structures have reached a high level of maturity: characterizations in terms of mesh topologies have been investigated [10], methods for compensating for numerical dispersion have been proposed [11], and a unified view of DWMs and wave digital filters [12] has been developed [13].

More recently, modal synthesis [14] has been applied to membrane simulation. Particularly relevant for the scope of this paper is the work by Rabenstein and coworkers [15], who have proposed the so-called functional transformation method (FTM): in essence, the method exploits the existence of an analytical form of the modal parameters for a set of relevant multidimensional differential systems, including strings and membranes with various boundary conditions. Finally, finite-difference methods have also been used, both for analysis [16], [17] and for synthesis purposes [18].

In their simplest formulation, physical models of membranes assume linearity of vibrations. However, this assumption can be accepted in the most coarse approximations only, and realistic models require abandoning it. Relevant nonlinearities include those involved in the excitation mechanisms (e.g., the impact force in hammer-membrane contact), as well as those arising at large amplitude membrane vibrations. This latter geometrical nonlinear effect occurs because in the large oscillation regime the membrane area, and thus its tension, are modulated in dependence of the instantaneous displacement. This produces an increase of the oscillation frequency at large displacements, and consequently frequency glides.

Manuscript received March 31, 2009; revised September 07, 2009. Current version published April 14, 2010. The associate editor coordinating the review of this manuscript and approving it for publication was Prof. Vesa Välimäki.

The authors are with the Dipartimento Ingegneria dell'Informazione, University of Padova, 35129 Padova, Italy (e-mail: avanzini@dei.unipd.it; marognar@dei.unipd.it).

Color versions of one or more of the figures in this paper are available online at http://ieeexplore.ieee.org.

Digital Object Identifier 10.1109/TASL.2009.2036903

This effect is audible in many instruments and characterizes strongly their timbre; therefore, it needs to be simulated in the synthesis models. Tension modulation in 1-D systems, i.e., strings, has been modeled in the context of both waveguide [19] and modal [20] approaches. Nonlinear extensions of the FTM have been proposed to include tension modulation effects, for the string [21] and the rectangular membrane [22]. More general nonlinear models of large amplitude vibrations of membranes can be derived from thin plate theories [23], [24], which account not only for pitch glides encountered in membranes, but also for more complex phenomena such as buildup of high-frequency energy and subharmonic generation exhibited, e.g., by cymbals and gongs [25], [26].

Quite surprisingly, given their relevance for musical applications, models for tension modulation in circular membranes are less studied than in rectangular ones. Moreover, other relevant sound production mechanisms in membrane percussions seem to have been so far largely disregarded in the literature of physical models. In this paper, we propose a physical model for tension modulation effects in a circular membrane, which is based on the so-called Berger approximation of the von Karman theory of thin plates [27]. It is shown that the model can be regarded as a 2-D extension of the tension-modulated string, and that it can be efficiently integrated into a modal synthesis engine. The nonlinear membrane is coupled to a nonlinear lumped model of impact force [28]. We then propose novel models for two relevant sound production mechanisms, i.e., membrane coupling through enclosed air in two-headed instruments, and string-membrane coupling. This latter sound production mechanism is encountered in several membrane percussions, starting from medieval and renaissance instruments like the tabor, up to marching instruments used in the military and modern orchestral instruments [1, Ch. 18], [29, Ch. 10].

We follow a modular approach in which individual elements (circular membrane, impact force, shell, and head coupling through air, additional interacting elements) are modeled separately, and can be subsequently combined to form different instruments. The topic of block-based modeling for physically based sound synthesis algorithms has received considerable attention in recent years [30], particularly for cases where different components may be modeled according to different paradigms. The models discussed in this paper are all based on a "lumped" approach, and interconnections are therefore straightforward.

Numerical realizations for all the models are derived using a general technique for the computation of nonlinear digital filter networks, recently proposed in [31]. Results from numerical simulations show that the models are able to capture the most relevant effects of the simulated physical mechanisms on the tone character: glides of partials due to tension modulation, occurrence of mode pairs due to coupling of two membranes, noisy oscillations due to string-membrane interaction.

The remainder of the paper is organized as follows. Section II summarizes a baseline physical model for a struck linear membrane [15]. This model is extended in Section III in order to account for nonlinear tension modulation effects, and a discrete-time formulation is proposed. Section IV discusses a model for simulating the effects of air loading and coupling of membranes in a percussion with two heads. Finally, a model for the simulation of string-membrane coupling is discussed in Section V. Results from numerical simulations of all the models are reported in Section VI. Accompanying audio examples can be found at http://smc.dei.unipd.it/membranes.html.

II. Struck Linear Circular Membrane

A. PDE for the Circular Membrane

The partial differential equation (PDE hereafter) that describes the vibration of a circular membrane with dispersion, dissipation, and driving force can be written as follows [32]:

$$D\nabla^4 z(r,\varphi,t) + \sigma\frac{\partial^2 z(r,\varphi,t)}{\partial t^2} - T_0\nabla^2 z(r,\varphi,t) + d_1\frac{\partial z(r,\varphi,t)}{\partial t} + d_3\frac{\partial \nabla^2 z(r,\varphi,t)}{\partial t} = f^{(\mathrm{ext})}(r,\varphi,t) \quad (1)$$

where $z(r,\varphi,t)$ is the membrane vertical displacement at the point (r,φ) (in polar coordinates) and time t, while $f^{(\mathrm{ext})}(r,\varphi,t)$ is the driving force density (in $\mathrm{N/m^2}$). The operators ∇^2 and $\nabla^4 = \nabla^2 \cdot \nabla^2$ are the Laplacian and biharmonic operator, respectively. The constants T_0 and σ are the membrane surface tension (in N/m) and surface density (in $\mathrm{Kg/m^2}$), and the corresponding wave velocity is $c = \sqrt{T_0/\sigma}$. Dissipation is modeled through a frequency-independent term d_1 and a frequency-dependent term d_3, which incorporate air losses, those inside the membrane, and those at the boundary [32]. Finally, the fourth-order term accounts for the effect of the (small) membrane bending stiffness $D = Eh^3/12(1-\upsilon^2)$, where h is the membrane height and E, υ are the material Young modulus and Poisson ratio, respectively.

The PDE has a unique solution given boundary and initial conditions. If $\mathcal{B} = \{(r,\varphi) : r = R\}$ is the circular boundary of a membrane with radius R, then ideal boundary conditions are represented by zero deflection and skewness on $\mathcal{B}$

$$z(r,\varphi,t)|_{(r,\varphi)\in\mathcal{B}} = 0, \quad \nabla^2 z(r,\varphi,t)|_{(r,\varphi)\in\mathcal{B}} = 0. \quad (2)$$

For the sake of simplicity, we choose the initial conditions in order to have zero initial displacement and zero initial velocity

$$z(r,\varphi,t)|_{t=0} = 0, \quad \left.\frac{\partial z(r,\varphi,t)}{\partial t}\right|_{t=0} = 0. \quad (3)$$

B. Normal Modes

The PDE in (1) can be turned into a set of ordinary differential equations that describe the dynamics of the normal modes. Recall that a mode is a particular solution of the PDE of the form $\bar{z}(t)K(r,\varphi)$, in which temporal and spatial dependencies are decoupled. The modal solution is associated to a Sturm–Liouville (SL) transform, an integral operator whose kernel is given by the spatial eigenfunctions K, i.e., the modal shapes. Clearly the kernel depends on the particular problem in exam: for the circular membrane with fixed boundary, it is known [1] that the corresponding spatial eigenfunctions are

$$K_{n,m}(r,\varphi) = \cos(n\varphi) J_n\left(\mu_{n,m}\frac{r}{R}\right) \quad (4)$$

where $n = 0,\ldots,+\infty, m = 1,\ldots,+\infty$, and $\mu_{n,m}$ is the mth zero of the nth-order Bessel function of the first kind, J_n. The

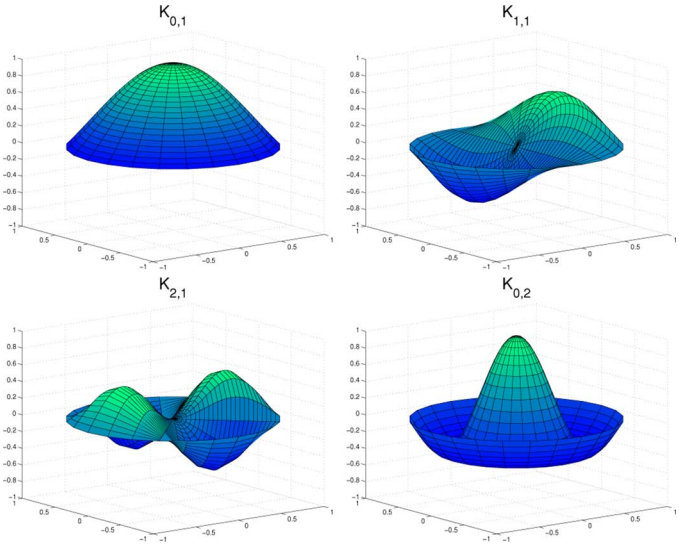

Fig. 1. Spatial eigenfunctions $K_{n,m}(r,\varphi)$ corresponding to the four lowest modal frequencies (the radial coordinate is normalized in all plots).

eigenfunctions corresponding to the lowest modal frequencies are shown in Fig. 1. The SL transform $\bar{g}$ of a generic function g and the inverse SL transform of $\bar{g}$ are then defined as

$$\bar{g}_{n,m}(t) = \int_0^{2\pi}\int_0^R g(r,\varphi,t)K_{n,m}(r,\varphi)\, r dr d\varphi.$$
$$g(r,\varphi,t) = \sum_{n=0}^{+\infty}\sum_{m=1}^{+\infty}\frac{\bar{g}_{n,m}(t)K_{n,m}(r,\varphi)}{\|K_{n,m}(r,\varphi)\|_2^2}. \quad (5)$$

The second equation in (5) expresses $g(r,\varphi,t)$ as the series of its normal modes $\bar{g}_{n,m}(t)$. By substituting the normal mode solution $z = \sum_{n,m}\bar{z}_{n,m}K_{n,m}/\|K_{n,m}\|_2^2$ in (1), and applying the SL transform, one finds the ordinary differential equations

$$\ddot{\bar{z}}_{n,m}(t) + \frac{1}{\sigma}\left[d_1 + d_3\left(\frac{\mu_{n,m}}{R}\right)^2\right]\dot{\bar{z}}_{n,m}(t) + \left(\frac{\mu_{n,m}}{R}\right)^2\left[\frac{D}{\sigma}\left(\frac{\mu_{n,m}}{R}\right)^2 + c^2\right]\bar{z}_{n,m}(t) = \frac{1}{\sigma}\bar{f}_{n,m}^{(\mathrm{ext})}(t). \quad (6)$$

Equation (6) says that the mode $\bar{z}_{n,m}$ is a forced second-order oscillator whose parameters are uniquely determined by those of the original PDE (an equivalent formulation can be found in [15]). The forcing term $\bar{f}_{n,m}^{(\mathrm{ext})}$ is the SL transform of $f^{(\mathrm{ext})}$

$$\bar{f}_{n,m}^{(\mathrm{ext})}(t) = \int_0^{2\pi}\int_0^R f^{(\mathrm{ext})}(r,\varphi,t)K_{n,m}(r,\varphi)\, r dr d\varphi. \quad (7)$$

In the ideal case of an external force (e.g., an impact force) applied at a single "hit" point $x_h = (r_h,\varphi_h)$ of the membrane surface, the force density takes the form $f^{(\mathrm{ext})}(r,\varphi,t) = F_h(t)\delta_{x_h}^2(r,\varphi)$, where the notation $\delta_{x_h}^2(\cdot)$ designates a 2-D Dirac function centered at x_h (more precisely, if $x = (r,\varphi)$, then $\delta_{x_h}^2(x) = \delta(|x - x_h|)/\pi|x - x_h|$.

Then (7) becomes

$$\bar{f}_{n,m}^{(\mathrm{ext})}(t) = F_h(t)K_{n,m}(r_h,\varphi_h). \quad (8)$$

C. Impact Force

The force density $f^{(\mathrm{ext})}$ that drives the membrane displacement in (1) may result from any kind of mechanical interaction. Since almost all membrane percussions are played by striking, we extend the linear membrane model with an impact model that describes the action of an ideal "hammer", e.g., a wooden stick or a mallet.

Assume that the hammer is a rigid body of mass m_h that moves with a trajectory $z_h(t)$. The hammer is hitting the membrane at the hit point $x_h = (r_h,\varphi_h)$ if its displacement is lower than the membrane displacement at x_h, i.e., if the condition $\zeta(t) = z(r_h,\varphi_h,t) - z_h(t) \geq 0$ holds. Then the force generated at the impact in x_h is given by

$$F_h(\zeta(t),\dot{\zeta}(t)) = \begin{cases} k\zeta(t)^\alpha + \lambda\zeta(t)^\alpha\dot{\zeta}(t), & \zeta > 0, \\ 0, & \text{otherwise} \end{cases} \quad (9)$$

where the parameter k is the force stiffness, λ is the force dissipation coefficient, and the exponent α depends on the local geometry around the contact area.

This model has been originally proposed in [33], and has been previously used in physically based models of contact sounds [28]. It can be regarded as an extension of the Hertz theory of contact, that includes non-spherical contact geometries, and accounts for dissipation during contact.

In the simplifying hypothesis of the force acting ideally on a single hit point, the impact model (9) can be straightforwardly coupled to the membrane model through (8). A more realistic approach [16] would require to estimate the average contact area and an associated spatial window $w_{x_h}(r,\varphi)$ around the hit point, so that $f^{(\mathrm{ext})}(r,\varphi,t) = F_h(t)w_{x_h}(r,\varphi)$ and $\bar{f}_{n,m}^{(\mathrm{ext})}$ can be computed to using the general (7).

If no other forces act on the hammer, its trajectory is coupled to the impact model through the Newton law $m_h\ddot{z}_h = F_h$. Note that since F_h depends on both the membrane and the hammer displacements, the complete model becomes nonlinear. This point is discussed further in Section III-C.

III. Nonlinear Membrane With Tension Modulation

The model described so far does not account for a very important nonlinear effect encountered in real membranes, i.e., tension modulation. Since the membrane area varies during oscillation, the tension also varies in dependence of the displacement, causing variations of the frequency content during the sound evolution, which become noticeable for large amplitude vibrations. Being tension modulation a geometrical nonlinearity (i.e., it only depends on the geometry of the problem, while the linear theory of elasticity is still assumed to hold), relatively simple models can be used to describe it.

A. Simplified Description of Large Amplitude Vibration

Nonlinear theories for large amplitude vibrations of membranes are typically derived from more general theories for thin plates subjected to lateral and in-plane forces [23], [24]. One

of the most widely used theories is due to von Karman [27]. In this approach, plate vibrations are modeled by means of two nonlinearly coupled PDEs, for transverse displacement and for a stress function. The von Karman equations have been applied to the sound synthesis of plates in [25] and [26].

A simpler approach to the modeling of geometrical nonlinearities in plates is that of Berger [34], [27]: it is based on a simplification of the von Karman equations, in which the elastic energy due to the second invariant of the membrane strain is disregarded compared to the square of the first invariant. A fundamental consequence of Berger approximation is that the resulting plate equations, although still nonlinear, are decoupled, which simplifies considerably the analysis.

The Berger approximation has no fully satisfactory justification, and may appear to be a mathematical device artificially introduced to decouple the problem. In fact, it has been shown to provide erroneous results for some boundary conditions, particularly when the plate edge is free to move in the in-plane direction. On the other hand, Berger equations provide accurate results for plates with clamped edges, and it has been demonstrated [35] that in this case the equations can be derived through a perturbation analysis method of the plate equations, without using the original Berger approximation. In particular, the model has been applied to the analysis of large amplitude deflection of membranes in [36], and has been shown to provide results that are in good agreement with other approximate analysis. As far as sound synthesis is concerned, it is noted in [25] that the Berger model is able to simulate the pitch gliding effects under exam here, although it cannot account for more dramatic nonlinear effects occurring in plates such as cymbals and gongs.

In light of the above discussion, we resolve to use the Berger model to simulate tension modulation effects in the circular membrane. The model can be formulated as follows:

$$D\nabla^4 z + \sigma\frac{\partial^2 z}{\partial t^2} - [T_0 + T_{\mathrm{NL}}(z)]\nabla^2 z + d_1\frac{\partial z}{\partial t} + d_3\frac{\partial \nabla^2 z}{\partial t} = f^{(\mathrm{ext})} \quad (10)$$

where we have omitted spatial and temporal dependencies for simplicity. The function $T_{\mathrm{NL}}(z)$ has the form [27]

$$T_{\mathrm{NL}}(z) = \frac{Eh}{2\pi R^2(1-\upsilon^2)} \cdot \int_0^R \int_0^{2\pi} \left[\left(\frac{\partial z}{\partial r}\right)^2 + \frac{1}{r^2}\left(\frac{\partial z}{\partial \varphi}\right)^2\right] r d\varphi dr. \quad (11)$$

According to these equations, the nonlinear term $T_{\mathrm{NL}}(z)$ is modeled as an integral over the state of the membrane, and can be interpreted as the surface tension generated in dependence of the displacement z, in addition to the tension at rest T_0.

Moreover, the double integral in (11) can be interpreted as a measure of the total membrane area corresponding to the displacement z. Specifically, Fig. 2 shows that a first order approximation of the infinitesimal area element dA is

$$dA \sim r\sqrt{1+\left(\frac{\partial z}{\partial r}\right)^2}\sqrt{1+\frac{1}{r^2}\left(\frac{\partial z}{\partial \varphi}\right)^2} dr d\varphi \sim dA_0 + \frac{1}{2}\left[\left(\frac{\partial z}{\partial r}\right)^2 + \frac{1}{r^2}\left(\frac{\partial z}{\partial \varphi}\right)^2\right] r dr d\varphi. \quad (12)$$

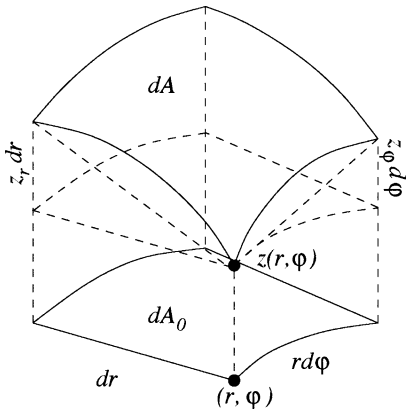

Fig. 2. Computation of area element dA as a function of the displacement $z(r,\varphi)$ [see (12)].

Therefore, the double integral in (11) is an estimate of the quantity $2[A(z) - A_0]$, where $A(z)$ is the total membrane area corresponding to the displacement z, and $A_0 = \pi R^2$ is the total area at rest. In this respect, the Berger model can be thought of as a 2-D extension of the Kirchhoff–Carrier model for the tension-modulated string (see, e.g., [1]).

B. Modal Formulation

If the nonlinear term that accounts for tension modulation in (10) is moved to the right-hand side, the resulting equation can be regarded as describing a linear membrane with constant tension T_0, which is forced by two excitation terms, $f^{(\mathrm{ext})}$ and $f^{(\mathrm{tm})}(z) = T_{\mathrm{NL}}(z)\nabla^2 z$. Both these terms are nonlinear and act in feedback to the membrane system, since they both depend on the membrane state.

In order to include $f^{(\mathrm{tm})}$ in the modal formulation, this has to be written in terms of the modes $\bar{z}$ rather than the displacement z. By applying the Sturm–Liouville transform, the nonlinear term in the transformed domain is then (see Appendix A)

$$\bar{f}^{(\mathrm{tm})}_{n,m}(\bar{z}, z) = -\left(\frac{\mu_{n,m}}{R}\right)^2 T_{\mathrm{NL}}(z)\bar{z}_{n,m} \quad (13)$$

and represents the effect of tension modulation on the (n,m) mode. In order to express $\bar{f}^{(\mathrm{tm})}_{n,m}$ as a function of the modes $\bar{z}$ only, the nonlinear tension $T_{\mathrm{NL}}(z)$ has to be rewritten as a function of $\bar{z}$. Substitution of the inverse SL transform (5) into (13) yields

$$\bar{T}_{\mathrm{NL}}(\bar{z}) = \frac{Eh}{2\pi R^2(1-\upsilon^2)} \int_0^R \int_0^{2\pi} \left[\left(\frac{\partial}{\partial r}\sum_{n,m}\frac{\bar{z}_{n,m}K_{n,m}}{\|K_{n,m}\|_2^2}\right)^2 + \frac{1}{r^2}\left(\frac{\partial}{\partial \varphi}\sum_{n,m}\frac{\bar{z}_{n,m}K_{n,m}}{\|K_{n,m}\|_2^2}\right)^2\right] r d\varphi dr. \quad (14)$$

The integral can be computed explicitly by exploiting the orthogonality of the functions $\cos(n\varphi)$, and the recurrence properties of the Bessel functions. The final result is

$$\bar{T}_{\mathrm{NL}}(\bar{z}) = \frac{Eh}{4R^2(1-\upsilon^2)} \cdot \sum_{n,m}\frac{\mu_{n,m}^2\bar{z}_{n,m}^2}{\|K_{n,m}\|_2^2}. \quad (15)$$

Details about the derivation are reported in Appendix B.

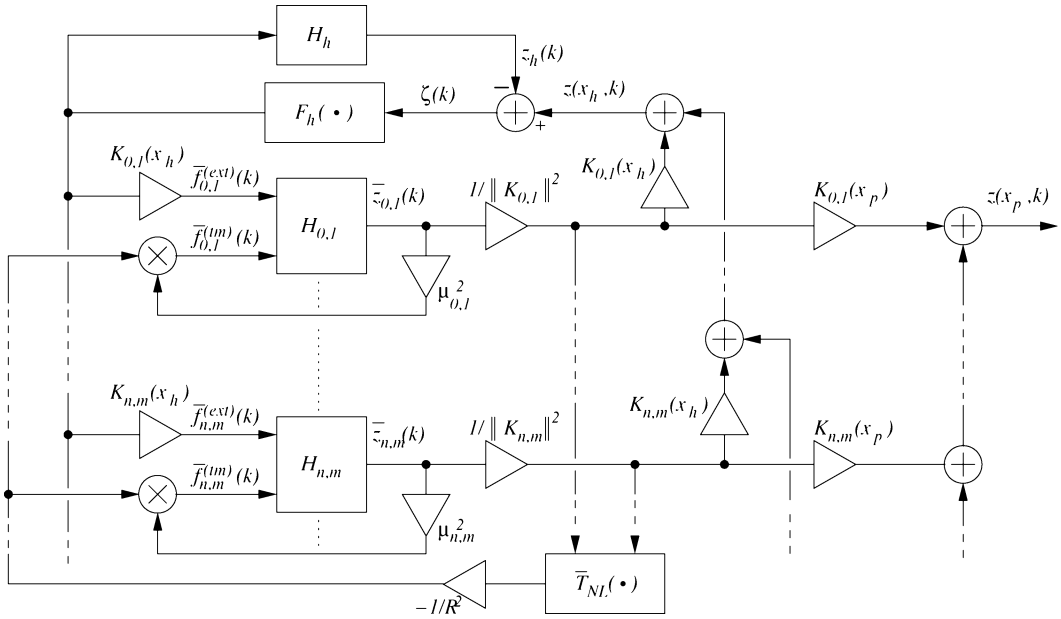

Fig. 3. Block scheme for the discrete-time realization of the nonlinear membrane model, including tension modulation and impact force. The integer $k \geq 0$ is the discrete time variable.

By means of (13), (15), a numerical realization of the nonlinear membrane can be developed in which $\bar{f}^{(\mathrm{tm})}_{n,m}$ is computed at runtime as a function of the outputs of the filter bank representing the modes, as explained in Section III-C next.

C. Numerical Realization

In the previous sections, the struck, tension-modulated membrane has been modeled as a liner membrane forced by the two excitation terms $f^{(\mathrm{ext})}$ and $f^{(\mathrm{tm})}$. Both these terms are algebraic (i.e., memoryless) nonlinearities, which depend on the membrane (and hammer) state.

The numerical realization is then based on the modal formulation of the linear membrane. From (6) one can see that in the Laplace domain the (n,m) normal mode is the output of a second-order filter $H_{n,m}(s)$, where

$$H_{n,m}(s) = \frac{\sigma^{-1}}{s^2 + 2\alpha_{n,m}s + \omega^2_{n,m}} \tag{16}$$

and where the loss factor $\alpha_{n,m}$ and the center frequency $\omega_{n,m}$ depend on the PDE parameters as follows:

$$\begin{aligned} 2\alpha_{n,m} &= \frac{1}{\sigma}\left[d_1 + d_3\left(\frac{\mu_{n,m}}{R}\right)^2\right], \\ \omega^2_{n,m} &= \left(\frac{\mu_{n,m}}{R}\right)^2\left[\frac{D}{\sigma}\left(\frac{\mu_{n,m}}{R}\right)^2 + c^2\right]. \end{aligned} \tag{17}$$

The filters are discretized using the bilinear transform, which has several desirable properties: it is a low-order method, and consequently the numerical filters are still second-order; it is an unconditionally stable numerical method; it is aliasing free. On the other hand, it introduces frequency warping, and consequently prewarping has to be applied to the resonators (16) when $\omega_{n,m}$ approaches a relevant fraction of the Nyquist frequency. However it has to be noted that warping becomes significant only if several hundreds of modes are simulated: as an example, for a membrane with $\omega_{0,1} = 2\pi \cdot 150$ rad/s and $N = M = 15$ nodal diameters and circles (i.e., 240 modes), the maximum modal frequency $\omega_{N,M} \simeq 4$ kHz is warped by less than 3% at a sampling rate $F_s = 44.1$ kHz. Moreover, higher modes are extremely dense and decays out quickly, so that they are perceived as high-frequency content especially in the attack transients, rather than individual spectral lines.

Similarly to the membrane modes, the hammer displacement z_h is the output of a second-order filter $H_h(s)$ applied to the impact force. If no other forces act on the hammer, the filter is

$$H_h(s) = \frac{m_h^{-1}}{s^2} \tag{18}$$

which is also discretized by means of the bilinear transform. In conclusion, $H_{n,m}$ and H_h are turned into numerical filters that are parametrically controlled through the membrane and hammer physical parameters.

The block scheme in Fig. 3 shows a numerical realization of the circular membrane. The bank of oscillators $H_{n,m}$ simulates a set of membrane modes, while the block H_h accounts for the dynamics of the hammer. The remaining blocks compute the nonlinear excitation signals. The impact force applied at the hit point x_h is computed in the block F_h as a function of hammer and membrane states, according to (9), and is fed back to the modes according to (8). The nonlinear tension is computed as a function of the modal displacements in the block $\bar{T}_{\mathrm{NL}}$, according to (15), and is fed back to the modes according to (13).

The input to the synthesis algorithm is represented by the initial hammer velocity (which corresponds to setting an appropriate initial state to the filter H_h) and by the hit point x_h. Initialization of H_h triggers the computation, and the system evolves autonomously until a subsequent impact is triggered, possibly at a different hit-point. The system output is taken to be the membrane displacement signal $z(x_p,k)$, captured at one (or possibly more) "pick-up" point x_p, which may or may not

coincide with the hit point. The signal $z(x_p, k)$ is the combination of the modes at x_p, according to (5).

The block scheme of Fig. 3 also shows that the computation of the forcing terms $\bar{f}_{n,m}^{(\mathrm{ext})}$, $\bar{f}_{n,m}^{(\mathrm{tm})}$ introduces feedback loops. Moreover, since these terms depend nonlinearly on instantaneous values of the modal displacements $\bar{z}_{n,m}$, delay-free computational loops are generated in the block scheme, and a nonlinear implicit system must be solved at every computation step in order to find new values of all system variables.

A general technique for the computation of nonlinear digital filter networks containing delay-free loops has been recently proposed in [31]. The method can be applied to digital networks composed of m_{NL} nonlinear and m_L linear discrete-time filters, arranged in an arbitrary topology. Delay-free loops are identified and solved through an *ad-hoc* iterative approach. In this case, the number of linear blocks m_L in the network coincides with the number $(N+1)\cdot M$ of simulated modes plus 1 (the filter H_h), while the number of nonlinear blocks coincides with the number of modes to which tension modulation is applied, plus 2 (the F_h and the T_{NL} blocks). The formalism and the numerical solver described in [31] can then be straightforwardly applied to the block scheme of Fig. 3.

IV. Shell, Air Cavity, Membrane Coupling

As discussed in the introduction, many membrane percussions consist of one head coupled to an air cavity, or two heads coupled through an air cavity. The air, and the shell in which it is enclosed, have two main effects: to provide an impedance to the membrane, and to radiate sound. From the modeling standpoint, it is convenient to treat separately these two effects, similarly to what is done in physical models of the piano soundboard [37].

A. A Simple Model of Air Cavity

Previous work [38] suggests that the role of the shell in radiating sound is negligible with respect to the membrane: although resonances can result from coupled motion of membrane and shell, and an appreciable amount of energy is associated with the shell motion, nonetheless most of the sound is radiated by the membrane. In the remainder of this section we do not consider coupling and radiation associated to the shell, which is treated as a perfectly rigid boundary. Instead we focus on the effects of the air enclosed in the shell, which affects the resulting sound through three mechanisms.

- For non-axisymmetric modes (modes (n,m) possessing nodal diameters, i.e., with $n>0$) it acts as an inertive load: mode oscillation does not compress the air in the cavity, but the effective modal mass is increased by the air mass, resulting in a lowering of the mode frequency.
- For axisymmetric modes $(n=0)$ it acts as an added stiffness: in this case the motion of the membrane changes the air volume, and the effective stiffness of the enclosed air will raise the mode frequency.
- For instruments composed of two heads, it couples heads especially at low frequencies: through this mechanism the vibration of the batter head is transmitted to the resonating carry head; in particular mode doublets will be generated when the two membranes have similar characteristics and tuning.

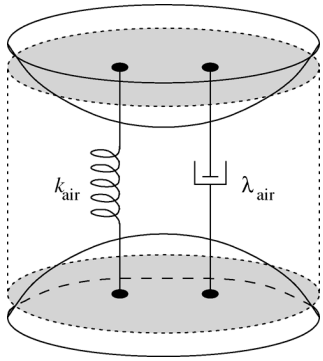

Fig. 4. Air coupling modeling for the mode (0, 1) through a simple spring/damper system.

The first effect can be straightforwardly incorporated into the membrane model by increasing the masses of the non-axisymmetric modes by an equivalent mass which takes into account the air load on the membrane surface (this effect is qualitatively similar to the air loading effect that is responsible for resonance tuning, e.g., in the orchestral timpani [39]). Analogously, the second effect can be incorporated into the model by increasing the stiffness of the non-axisymmetric modes. However the most interesting effect is the third one, since coupling of the two heads affects significantly the sound timbre.

The model proposed here is based on a lumped approach and consists of a spring/damper system coupled to both heads. Since the air load is distributed over the membrane surface, we model air-membrane interaction as a constant force density applied to the whole membrane surface (as depicted in Fig. 4 for the (0, 1) mode). Therefore, the coupling effect is mainly noticeable for the modes of type $(0,m)$, and especially the (0, 1) mode. On the other hand, modes (n,m) with $n>0$ remain unaffected by air coupling since these modes produce null net displacement of the surrounding air, due to the symmetric configuration of the nodal patterns ([40, Sec. 4.5]).

B. Realization

According to the spring/damper system described above, the corresponding equation for the resulting force is

$$F_{\mathrm{air}}(t) = k_{\mathrm{air}}[\hat{z}_1(t) - \hat{z}_2(t)] + \lambda_{\mathrm{air}}[\dot{\hat{z}}_1(t) - \dot{\hat{z}}_2(t)] \qquad (19)$$

where $\hat{z}_{1,2}$ are the average displacements of the two membranes, $k_{\mathrm{air}}, \lambda_{\mathrm{air}}$ are the air spring stiffness and dissipation term, respectively. The average membrane displacement $\hat{z}$ is defined as the sum of the average modal displacements

$$\hat{z}(t) = \sum_{n=0}^{+\infty}\sum_{m=1}^{+\infty} \bar{z}_{n,m}(t)\frac{\int_0^{2\pi}\int_0^R K_{n,m}(r,\varphi)rdrd\varphi}{\pi R^2 \|K_{n,m}(r,\varphi)\|_2^2}. \qquad (20)$$

The coupling force F_{air} has to be applied on each membrane surface through a corresponding constant force density $f^{(\mathrm{air})}(t) = F_{\mathrm{air}}(t)/\pi R^2$. In the SL domain this force density translates into

$$\bar{f}_{n,m}^{(\mathrm{air})}(t) = f^{(\mathrm{air})}(t)\int_0^{2\pi}\int_0^R K_{n,m}(r,\varphi)\, rdrd\varphi. \qquad (21)$$

The kernel integral in (21) includes an integral of Bessel function of the type $\int_0^R J_n(\mu_{nm}(r/R))rdr$, which in general has no close solution. However, it also includes an integral of the type $\int_0^{2\pi}\cos(n\varphi)d\varphi$, which is non-null only for $n=0$ (i.e., the average modal displacement is non-null only for $n=0$, as already stated). In this particular case, a known property of Bessel functions can be used

$$\int x^n J_{n-1}(x)dx = x^n J_n(x), \quad (n>0). \tag{22}$$

Using this property, (21) is rewritten for modes $(0,m)$ as

$$\bar{f}_{0,m}^{(\mathrm{air})}(t) = f^{(\mathrm{air})}(t)\cdot\frac{2\pi R^2}{\mu_{0,m}}J_1(\mu_{0,m}) \tag{23}$$

while $\bar{f}_{n,m}^{(\mathrm{air})}=0$ for $n\neq 0$.

Equations (19), (20), and (23) form the air cavity model. The model can be straightforwardly integrated into the block scheme of Fig. 3, through the inclusion of an additional feedback loop in which 1) the average displacement $\hat{z}(k)$ is computed at each time instant k from the modal displacements $\bar{z}_{n,m}(k)$ with (20), and 2) the force $F_{\mathrm{air}}(k)$ is computed from $\hat{z}(k)$ with (19), and (c) the force components $\bar{f}_{0,m}^{(\mathrm{air})}(k)$ are computed with (23) and injected into the corresponding filters $H_{0,m}$.

Since $\bar{f}_{n,m}^{(\mathrm{air})}(k)=0$ for the modes with $n\neq 0$, the model does not account for the occurrence of doublets for these modes. This is apparently in contrast with some experimental results [38] where doublets are observed, e.g., for the mode (1, 1). However, these doublets are to be attributed to other mechanisms, such as mechanical coupling through the shell, or density and tension irregularities in the membranes [41].

V. Membrane–String Interaction

Several membrane percussion instruments make use of a distinguishing sound production mechanism, in which strands or cables of wire or gut are stretched across the membrane ([1, Sec. 18.10, 18.13], [29]. When the membrane is set into motion, it vibrates against the string producing a noisy sound. By virtue of this mechanism, such instruments belong to the family of untuned membranophones.

A. Lumped Model

Fig. 5(a) visualizes the simplest configuration of membrane-string interaction, such as that encountered in the medieval tabor [29]. For clarity this basic configuration is discussed here, and the proposed model can be straightforwardly extended to the case of multiple interacting strands on the membrane. We choose to follow a lumped modeling approach, in which the interaction is represented as point-like excitations on the membrane. A somewhat similar approach has been recently applied to the simulation of the prepared piano, in which preparation elements are modeled as lumped nonlinearities [42].

The string can make contact with the membrane on a very large number of points. A distributed string model based on waveguide structures or finite differences, that simulates contact with the membrane on such a large number of points, would require to pick up the membrane displacement in each of these points. However, this is a computationally expensive operation

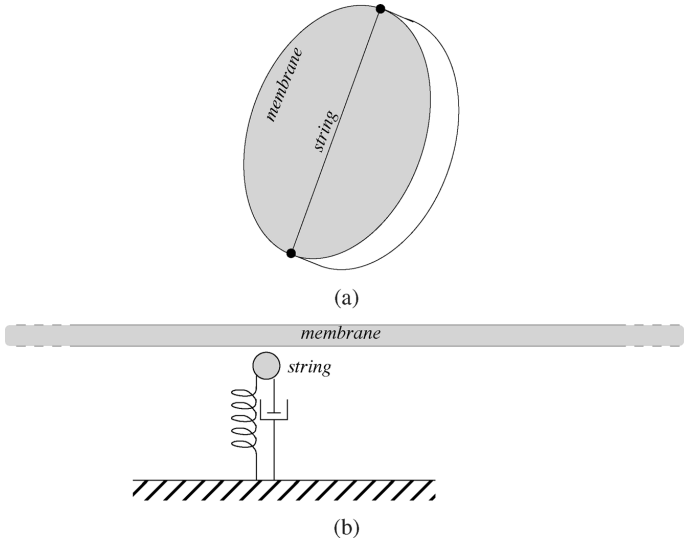

Fig. 5. String-membrane interaction. (a) Schematic visualization of a single string stretched across the membrane, and (b) a lumped model (the string extends perpendicularly to the plane of the figure).

in the modal synthesis framework used in this work, since it requires $N\cdot M$ multiplications and $N\cdot M$ additions for each pick-up point, where (N,M) is the order of the highest simulated mode (see Section III-C).

For this reason a different approach is followed, based on two simplifying assumptions. First, especially metallic strings used in certain percussions possess high bending stiffness and are extremely rigid. Second, string oscillations are usually very small, since it is set into motion by the membrane oscillation rather than through direct excitation. Therefore, we choose to consider a stiff modal string in which only the first mode of oscillation is considered.

The problem remains of how to choose the contact points. In order to keep the computational complexity low, it is assumed that the string makes contact with the membrane at the point of maximum displacement, i.e., at half the string length. Fig. 5(b) visualizes the model.

B. Realization

According to the model described above, the string displacement z_{st} obeys the PDE of a stiff string with dissipation

$$E_{\mathrm{st}}I_{\mathrm{st}}\frac{\partial^4 z_{\mathrm{st}}}{\partial r^4}+\mu_{\mathrm{st}}\frac{\partial^2 z_{\mathrm{st}}}{\partial t^2}-T_{\mathrm{st}}\frac{\partial^2 z_{\mathrm{st}}}{\partial r^2}+d_{\mathrm{st}}\frac{\partial z_{\mathrm{st}}}{\partial t}=f^{(\mathrm{st})} \tag{24}$$

where E_{st} and I_{st} are the Young modulus and moment of inertia, respectively ($I_{\mathrm{st}}=S_{\mathrm{st}}\kappa_{\mathrm{st}}^2$, where S_{st} is the string cross-section and κ_{st} is the radius of gyration, e.g., $\kappa_{\mathrm{st}}=a/2$ for a string with circular cross section and constant radius a). The parameters μ_{st} and T_{st} represent string linear density and tension, respectively, while d_{st} is the dissipation coefficient (we do not include a frequency dependent dissipation term since only the first mode is simulated). The forcing term $f^{(\mathrm{st})}$ is due to the impact force between string and membrane, which is simulated using the model (9) discussed in Section II-C.

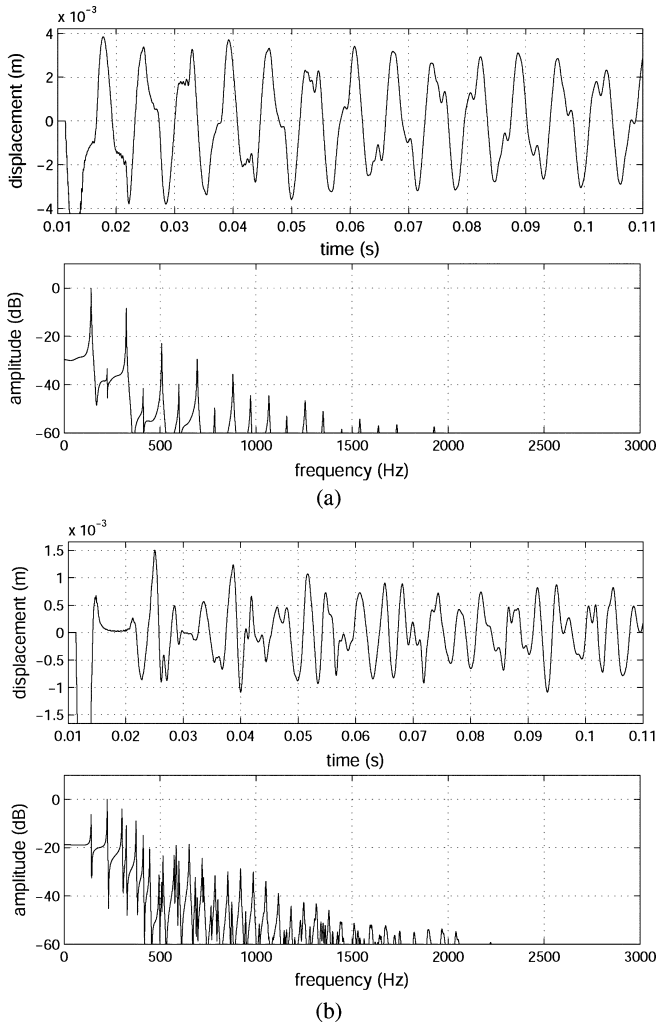

Fig. 6. Numerical simulations of a struck membrane with varying hit point. (a) Initial oscillation cycles of membrane displacement at the hit point (upper panel) and corresponding spectrum (lower panel) for $r_h = 0.05R$. (b) The same data for $r_h = 0.8R$.

A modal formulation for the string of (24) can be derived using the same approach described for the circular membrane in Section II-B, with the one-dimensional kernel functions $K_n(r) = \sin(n\pi(r/R))$. By applying the SL transform one finds [21] that the first mode of oscillation is modeled by the second-order mechanical oscillator

$$H_{\rm st}(s) = \frac{\mu_{\rm st}^{-1}}{s^2 + 2\alpha_{\rm st}s + \omega_{\rm st}^2} \tag{25}$$

where the loss factor $\alpha_{\rm st}$ and the center frequency $\omega_{\rm st}$ depend on the PDE parameters as follows:

$$2\alpha_{\rm st} = \frac{d_{\rm st}}{\mu_{\rm st}}, \quad \omega_{\rm st}^2 = \frac{\pi^2}{R^2}\left[\frac{E_{\rm st}I_{\rm st}\pi^2}{R^2} + c_{\rm st}^2\right] \tag{26}$$

where $c_{\rm st}^2 = T_{\rm st}/\mu_{\rm st}$. This oscillator is discretized with the same approach outlined in Section III-C for the oscillator (16), and is coupled to the membrane model through the interaction force F_h of (9).

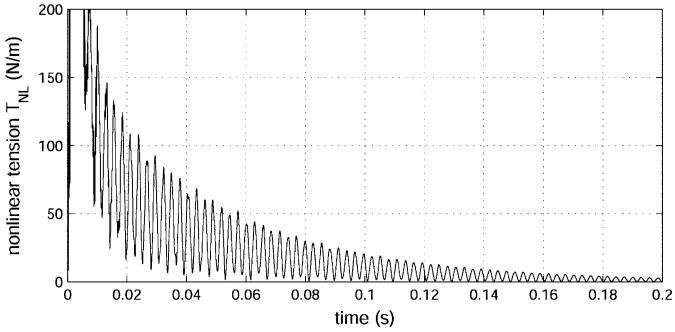

Fig. 7. Numerical simulations of the nonlinear membrane struck with high impact velocity: variation in time of $T_{\rm NL}$.

VI. Simulations

The numerical models discussed in the previous sections have been implemented in Matlab. This section discusses results from numerical simulations (accompanying audio examples can be found at http://smc.dei.unipd.it/membranes.html). The following values have been used in all simulations for the main physical parameters: $R = 16 - 20$ cm, $h = 0.2$ mm, $\sigma = 0.27$ Kg/m^2, $E = 3.5 \cdot 10^9$ Pa, $\upsilon = 0.2, d_1 = 1.25$ Kg/m^{2}s, $d_3 = 5 \cdot 10^{-4}$ Kg/s. The sample rate $F_s = 44.1$ kHz has always been used. The highest order (N, M) of the simulated modes has been varied from $N = M = 5$ to $N = M = 20$ depending on the desired accuracy, which corresponds to a maximum of $(N + 1) \cdot M = 420$ simulated modes.

A. Struck Membrane

Numerical simulations of the membrane model have been finalized at assessing the ability of the model to react consistently to different inputs (hit point and impact velocities), and particularly to simulate glides exhibited by real membranes.

Fig. 6 shows results from two simulations in which the membrane has been struck at two different hit points, and with the same impact velocity: in Fig. 6(a) x_h is close to the center ($r_h \sim 0$), while in Fig. 6(b) x_h is close to the rim ($r_h \sim R$). Both the time-domain oscillations and the corresponding spectra show that energy from the impact is transmitted mostly to the modes with lowest frequencies when the hit point is close to the centre, while higher modes are excited when the hit point is close to the rim. This behavior is qualitatively similar to that of a 1-D string, but is even more noticeable in the 2-D circular membrane, due to the much higher modal density. For a player, the influence of the hit point on the resulting sound spectrum is extremely important.

Fig. 7 shows a plot of the nonlinear tension $T_{\rm NL}$ as a function of time, obtained from a numerical simulation of the nonlinear membrane model of Fig. 3. In this case, the membrane has been struck near the center ($r_h = 0.1R$) with a high impact velocity. Being proportional to the total membrane area, the signal $T_{\rm NL}(t)$ oscillates twice as fast as the fundamental frequency of oscillation of the membrane. The effects of tension modulation on the resulting sound are illustrated in Fig. 8. The expected glides can be observed in the trajectories of the modal frequencies.

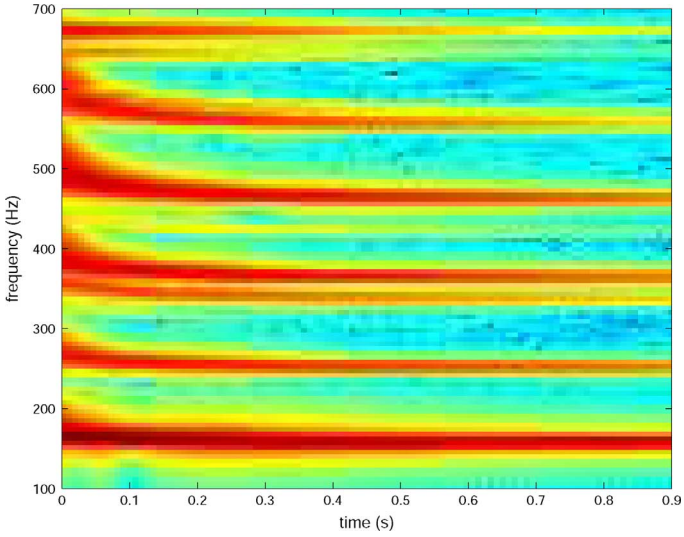

Fig. 8. Numerical simulations of a nonlinear membrane struck with high impact velocity: spectrogram of the resulting sound. The initial glides for the lower partials closely resemble those observed in a real membrane.

Apart from the impact velocity, the decay rate of T_{NL} is influenced mainly by the parameters $d_{1,3}$, because these parameters determine the decay times of the membrane modes. Moreover, the total number of modes involved in the sum (15) has also a major influence: using an insufficient number of modes produces an unnaturally slowly decaying tension. In the case of Figs. 7 and 8, $N = M = 15$ nodal diameters and circles have been simulated. With these values, the tension modulation and the corresponding modal frequency glides have a duration of a few tenths of seconds, and resemble closely those observed in real membranes [43].

B. Coupled Membranes

The coupling between the batter and carry heads produces different sound spectra depending on their relative tuning. In particular, if the linear tensions of the membranes are close, the resulting sound reveals as expected beatings that are due to mode doublets. On the other side, if the two tensions are well separated (as an example, the carry head may be tuned "one fourth" lower than the batter head), beatings do not occur but the frequency content of the carry head is injected into the batter head producing an overall richer spectrum.

Examples of these effects are illustrated in Fig. 9, which shows the displacement signal at a pick-up point of the carry head, and the corresponding spectrum, when the batter head is struck. The case of nearly identical tensions is exemplified in Fig. 9(a): since the frequencies of the (0, 1) modes are close, the displacement exhibits beating. The case of well separated tensions is exemplified in Fig. 9(b): no significant beating effect is observed, but the spectrum reveals that spectral energy has been injected from the batter to the carry head.

C. String-Membrane Interaction

The effect of the main string parameters (i.e., mass, tension, and dissipation) on the resulting sound has been investigated by performing "sweep tests" in which each of these parameters varied over a wide range.

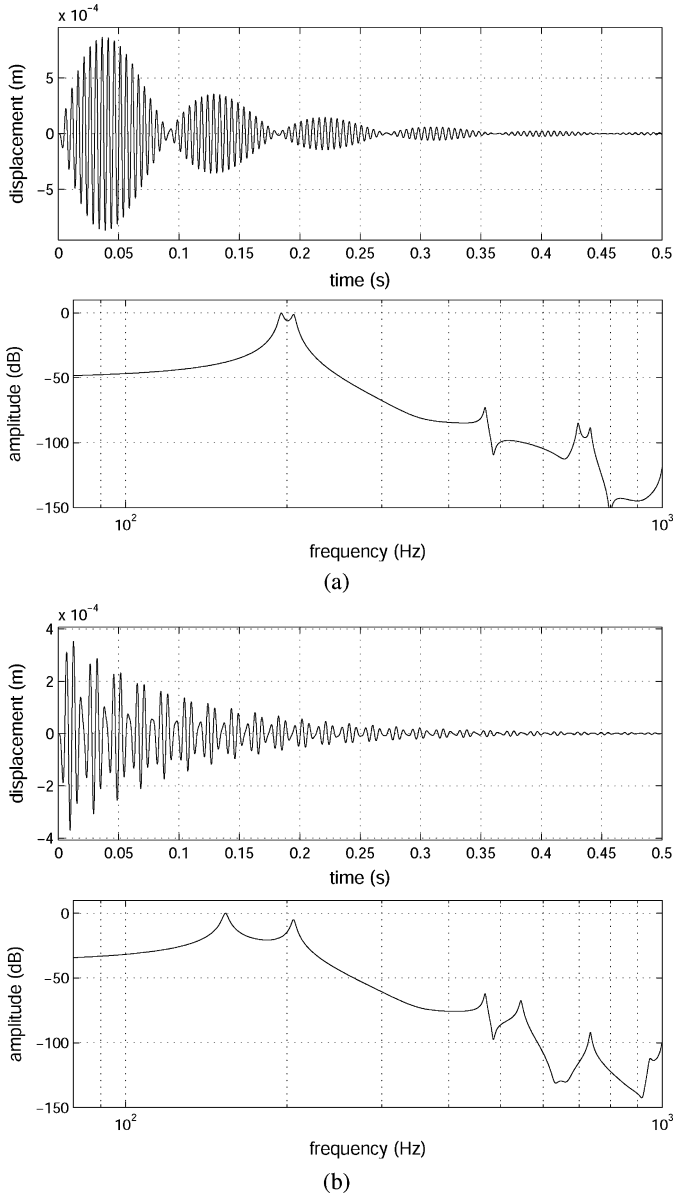

Fig. 9. Numerical simulations of two membranes coupled through air, with different values for the linear tensions $T_{1,2}$ of the batter and carry head, respectively. (a) Carry head displacement and corresponding spectrum for $T_2 \sim T_1$ ($T_1 = 2000$ and $T_2 = 1800$). (b) Carry head displacement and corresponding spectrum for $T_2 \ll T_1$ ($T_1 = 2000$ and $T_2 = 1100$).

Numerical simulations show that the string tension T_{st} is the one that affects most the resulting sound. At low values, string-membrane contacts are less dense in time: an example of this behavior is shown in Fig. 10(a). As T_{st} is increased, the proper string oscillation frequency is also increased, producing a higher density of contacts: an example of this behavior is shown in Fig. 10(b). Note that the simulated interaction depicted in Fig. 10 is qualitatively similar to that obtained from experimental measurements (see [1 Sec. 18.13]).

Consequently, T_{st} has a major effect on the brightness of the resulting sound, where brighter sounds result from higher stiffness values. This effect resembles the one obtained by changing the tension of the string on a real instrument.

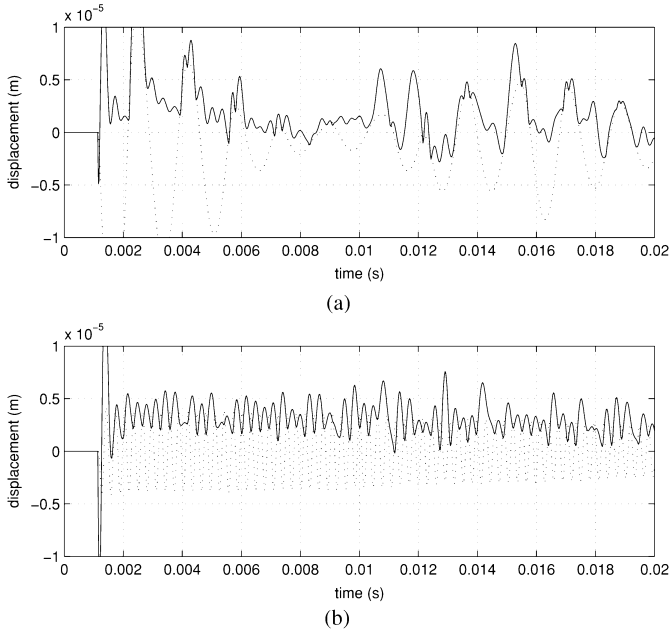

Fig. 10. Numerical simulations of string-membrane interaction. Membrane displacement (solid line) and string displacement (dotted line) with (a) low and (b) high string tension value.

VII. Conclusion

In this paper, a set of physical models for sound synthesis of membrane percussions was proposed. It was shown that tension modulation in a struck circular membrane can be simulated by a modal sound synthesis model, by including a nonlinear term that computes the time-varying tension as a function of the membrane displacement. Results from numerical simulations show that the model captures the most relevant effect of tension modulation, i.e., variations of frequencies of the membrane modes. Although the focus of the paper is not about exact resynthesis of sounds recorded from real membranes, it has been shown that proper choices of the geometrical and physical parameters of the membrane model result in sound spectra that resemble closely those observed in real circular membranes.

Novel models for two relevant sound production mechanisms were then proposed, i.e., membrane coupling through enclosed air in two-headed instruments, and string-membrane coupling. Both models are based on a lumped approach, and can therefore be straightforwardly connected in a modular fashion to the modal synthesis engine used for the membrane model.

Numerical simulations of a system composed by two membranes coupled through air show that, when the two membranes have similar tuning, strong coupling between the heads leads to the occurrence of doublets, which are especially noticeable in the low frequency range. However, the coupling model is still lacking many relevant features. In particular, we have not investigated the role of the shell in the coupling mechanism, nor the effect of the air cavity resonances in sustaining modes of oscillation in the membrane. Also in light of the scarce literature on the subject, the main coupling mechanisms will need to be further investigated by means of both acoustic/mechanical measurement, and finite-element simulations.

Numerical simulations of a system composed by a membrane and a string in interaction show that the simulated string action is qualitatively similar to that observed in experimental measurements. In particular, string tension is the parameter that affects most the resulting sound, with brighter sounds resulting from higher tension values. The proposed approach will need to be further validated in terms of both thorough comparisons with measurements on real instruments, and extensions to more complex configurations including multiple interacting strands.

Appendix A
Excitation Term $\bar{f}^{(\mathrm{tm})}_{n,m}(\bar{z})$

Here we prove (13) by calculating $\bar{f}^{(\mathrm{tm})}_{n,m}(\bar{z})$ as the SL transform of the excitation term $f^{(\mathrm{tm})}(z)$

$$\bar{f}^{(\mathrm{tm})}_{n,m}(\bar{z}) = T_{\mathrm{NL}}(z)\int_0^R\int_0^{2\pi} \nabla^2 z(r,\varphi) K_{n,m}(r,\varphi)\, r dr d\varphi \tag{27}$$

where the transformation kernel $K_{n,m}$ is given in (4). Integration by parts yields

$$\bar{f}^{(\mathrm{tm})}_{n,m}(\bar{z}) = T_{\mathrm{NL}}(z)\int_0^R\int_0^{2\pi} z(r,\varphi) \nabla^2 K_{n,m}(r,\varphi)\, r dr d\varphi. \tag{28}$$

From this, (13) would follow immediately by recalling that $K_{n,m}$ are the eigenfunctions of the operator ∇^2, with associated eigenvalues $-(\mu_{nm}/R)^2$. However, for the sake of clarity we provide an explicit derivation.

By recalling that $\nabla^2 = (\partial^2/\partial r^2) + (1/r)(\partial/\partial r) + (1/r^2)(\partial^2/\partial\varphi^2)$, the Laplacian $\nabla^2 K_{n,m}$ can be written as

$$\nabla^2 K_{n,m}(x,\varphi) = \cos(n\varphi)\left(\frac{\mu_{n,m}}{R}\right)^2 \cdot\left[\frac{\partial^2 J_n(x)}{\partial x^2} + \frac{1}{x}\frac{\partial J_n(x)}{\partial x} - \frac{n^2}{x^2} J_n(x)\right] \tag{29}$$

where we have also substituted the variable $x = \mu_{n,m}(r/R)$. Since Bessel functions satisfy the equation

$$x^2\frac{\partial^2 J_n(x)}{\partial x^2} + x\frac{\partial J_n(x)}{\partial x} + (x^2 - n^2) J_n(x) = 0 \tag{30}$$

the Laplacian (29) can be rewritten as

$$\nabla^2 K_{n,m}(r,\varphi) = -\left(\frac{\mu_{nm}}{R}\right)^2 K_{n,m}(r,\varphi). \tag{31}$$

Substituting this expression into (28) proves (13).

Appendix B
Nonlinear Tension $\bar{T}_{\mathrm{NL}}(\bar{z})$

Here we prove (15) by solving the integral in (14). First, by exploiting the orthogonality of the functions $\cos(n\varphi)$ (14) can be rewritten as

$$\bar{T}_{\mathrm{NL}}(\bar{z}) = \frac{Eh}{2\pi R^2(1-\upsilon^2)}\sum_{n,m}\frac{\bar{z}^2_{n,m}}{\|K_{n,m}\|_2^4}\int_0^R\int_0^{2\pi} r d\varphi dr \cdot\left[\cos^2(n\varphi)\left(\frac{dJ_n(\frac{\mu_{n,m}r}{R})}{dr}\right)^2 + \frac{n^2}{r^2}\sin^2(n\varphi) J_n^2\left(\frac{\mu_{n,m}r}{R}\right)\right]. \tag{32}$$

Second, by substituting the variable $x = \mu_{n,m}(r/R)$ the above equation becomes

$$\bar{T}_{\mathrm{NL}}(\bar{z}) = \frac{Eh}{2\pi R^2(1-\upsilon^2)} \sum_{n,m} \frac{\bar{z}_{n,m}^2}{\|K_{n,m}\|_2^4} \cdot \left[\int_0^{2\pi} \cos^2(n\varphi) d\varphi \int_0^{\mu_{n,m}} x \left(\frac{dJ_n(x)}{dx} \right)^2 dx + n^2 \int_0^{2\pi} \sin^2(n\varphi) d\varphi \int_0^{\mu_{n,m}} \frac{J_n^2(x)}{x} dx \right] \quad (33)$$

and finally

$$\bar{T}_{\mathrm{NL}}(\bar{z}) = \frac{Eh}{2\pi R^2(1-\upsilon^2)} \cdot \sum_{n,m} \frac{\pi(1+\delta_{n,0})\bar{z}_{n,m}^2}{\|K_{n,m}\|_2^4} \cdot \int_0^{\mu_{n,m}} \left[x \left(\frac{dJ_n(x)}{dx} \right)^2 + n^2 \frac{J_n^2(x)}{x} \right] dx \quad (34)$$

where the term $\pi(1+\delta_{n,0})$ accounts for the trigonometric integrals in (33) (and $\delta_{n,0}$ is the Kronecker delta). Now the integral above has to be calculated explicitely. To this end, first recall the recurrence properties of Bessel functions

$$J_{n-1}(x) + J_{n+1}(x) = \frac{2n}{x} J_n(x),$$
$$J_{n-1}(x) - J_{n+1}(x) = 2\frac{dJ_n}{dx}(x). \quad (35)$$

Using these relations the integrand function in (34) becomes

$$x \left(\frac{dJ_n(x)}{dx} \right)^2 + n^2 \frac{J_n^2(x)}{x} = \frac{x}{2} \left[J_{n-1}^2(x) + J_{n+1}^2(x) \right]. \quad (36)$$

Then, recall that in general

$$\int x J_n^2(x) dx = \frac{x^2}{2} \left[J_n^2(x) - J_{n-1}(x) J_{n+1}(x) \right]. \quad (37)$$

Using (36) and (37), the integral in (34) can be written as

$$\frac{1}{2} \int_0^{\mu_{n,m}} x \left[J_{n-1}^2(x) + J_{n+1}^2(x) \right] dx = \frac{\mu_{n,m}^2}{4} \left[J_{n-1}^2(\mu_{n,m}) + J_{n+1}^2(\mu_{n,m}) \right]. \quad (38)$$

Finally, observing that $J_{n-1}(\mu_{n,m}) = -J_{n+1}(\mu_{n,m})$, and that $\|K_{n,m}\|_2^2 = \pi R^2(1+\delta_{n,0}) J_{n+1}^2(\mu_{n,m})/2$, yields the encouragingly compact (15).

ACKNOWLEDGMENT

The authors are would like to thank S. Bilbao for his insightful remarks about the nonlinear membrane model and its relation with Berger equations. They would also like to thank B. Bank and S. Zambon for their helpful suggestions about the air cavity model described in Section IV.

REFERENCES

[1] N. H. Fletcher and T. D. Rossing, *The Physics of Musical Instruments*. New York: Springer-Verlag, 1991.

[2] J. Backus, "Effect of wall material on the steady-state tone quality of woodwind instruments," *J. Acoust. Soc. Amer.*, vol. 36, no. 10, pp. 1881–1887, Oct. 1964.

[3] J. W. Coltman, "Effect of material of flute tone quality," *J. Acoust. Soc. Amer.*, vol. 49, no. 2, pp. 520–523, 1971.

[4] J. O. Smith III, "Virtual acoustic musical instruments: Review and update," *J. New Music Res.*, vol. 33, no. 3, pp. 283–304, Autumn, 2004.

[5] V. Välimäki, J. Pakarinen, C. Erkut, and M. Karjalainen, "Discrete-time modelling of musical instruments," *Rep. Prog. Phys.*, vol. 69, no. 1, pp. 1–78, 2006.

[6] M. Sandler, "Analysis and synthesis of atonal percussion using high order linear predictive coding," *Appl. Acoust.*, vol. 30, no. 2–3, pp. 247–264, 1990.

[7] J. Laroche and J.-L. Meillier, "Multichannel excitation/filter modeling of percussive sounds with application to the piano," *IEEE Trans. Speech Audio Process.*, vol. 2, no. 2, pp. 329–344, Apr. 1994.

[8] P. R. Cook, "Physically informed sonic modeling (PhISM): Synthesis of percussive sounds," *Comput. Music J.*, vol. 21, no. 3, pp. 38–49, 1997.

[9] S. A. van Duyne and J. O. Smith III, "The 2-D digital waveguide mesh," in *Proc. IEEE Workshop Applicat. Signal Process. Audio Acoust. (WASPAA'93)*, New Paltz, NY, Oct. 1993, pp. 177–180.

[10] F. Fontana and D. Rocchesso, "Signal-theoretic characterization of waveguide mesh geometries for models of two-dimensional wave propagation in elastic media," *IEEE Trans. Speech Audio Process.*, vol. 9, no. 2, pp. 152–161, Feb. 2001.

[11] L. Savioja and V. Välimäki, "Interpolated rectangular 3-D digital waveguide mesh algorithms with frequency warping," *IEEE Trans. Speech Audio Process.*, vol. 11, no. 6, pp. 783–790, Nov. 2003.

[12] A. Fettweis, "Wave digital filters: Theory and practice," *Proc. IEEE*, vol. 74, no. 2, pp. 270–327, Feb. 1986.

[13] S. Bilbao, *Wave and Scattering Methods for Numerical Simulation*. Chichester: Wiley, 2005.

[14] J.-M. Adrien, "The missing link: Modal synthesis," in *Representations of Musical Signals*, G. De Poli, A. Piccialli, and C. Roads, Eds. Cambridge, MA: MIT Press, 1991, pp. 269–297.

[15] L. Trautmann and R. Rabenstein, *Digital Sound Synthesis by Physical Modeling Using the Functional Transformation Method*. New York: Kluwer, 2003.

[16] L. Rhaouti, A. Chaigne, and P. Joly, "Time-domain modeling and numerical simulation of a kettledrum," *J. Acoust. Soc. Amer.*, vol. 105, no. 6, pp. 3545–3562, Jun. 1999.

[17] A. Chaigne and C. Lambourg, "Time-domain simulation of damped impacted plates. Part I. Theory and experiments," *J. Acoust. Soc. Amer.*, vol. 109, no. 4, pp. 1422–1432, Apr. 2001.

[18] M. van Walstijn and K. Kowalczyk, "On the numerical solution of the 2D wave equation with compact fdtd schemes," in *Proc. Int. Conf. Digital Audio Effects (DAFx-08)*, Helsinki, Finland, Sep. 2008, pp. 205–212.

[19] T. Tolonen, V. Välimäki, and M. Karjalainen, "Modeling of tension modulation nonlinearity in plucked strings," *IEEE Trans. Speech Audio Process.*, vol. 8, no. 3, pp. 300–310, May 2004.

[20] S. Bilbao, "Modal type synthesis techniques for nonlinear strings with an energy conservation property," in *Proc. Int. Conf. Digital Audio Effects (DAFx-04)*, Naples, Italy, Oct. 2004, pp. 119–124.

[21] R. Rabenstein and L. Trautmann, "Digital sound synthesis of string instruments with the functional transformation method," *Signal Process.*, vol. 83, no. 8, pp. 1673–1688, Aug. 2003.

[22] S. Petrausch and R. Rabenstein, "Tension modulated nonlinear 2D models for digital sound synthesis with the functional transformation method," in *Proc. European Sig. Process. Conf. (EUSIPCO2005)*, Antalya, Turkey, Sep. 2005.

[23] C. H. Jenkins and J. W. Leonard, "Nonlinear dynamic response of membranes: State of the art," *Appl. Mech. Rev.*, vol. 44, no. 7, pp. 319–328, Jul. 1991.

[24] C. H. Jenkins, "Nonlinear dynamic response of membranes: State of the art-update," *Appl. Mech. Rev.*, vol. 48, no. 10, pt. 2, pp. S41–S48, Oct. 1996.

[25] S. Bilbao, "Sound synthesis for nonlinear plates," in *Proc. Int. Conf. Digital Audio Effects (DAFx-05)*, Madrid, Spain, Sep. 2005, pp. 243–248.

[26] S. Bilbao, "A family of conservative finite difference schemes for the dynamical von Karman plate equations," *Numer. Methods Partial Differential Eq.*, vol. 24, no. 1, pp. 193–216, 2008.

[27] J. S. Rao, *Dynamics of Plates*. New York: CRC, 1998.

[28] F. Avanzini, M. Rath, D. Rocchesso, and L. Ottaviani, "Low-level sound models: Resonators, interactions, surface textures," in *The Sounding Object*, D. Rocchesso and F. Fontana, Eds. Florence, Italy: Mondo Estremo, 2003, pp. 137–172.

[29] J. Blades, *Percussion Instruments and Their History*, 4th ed. London, U.K.: Kahn & Averill, 1993.
[30] R. Rabenstein, S. Petrausch, A. Sarti, G. D. Sanctis, C. Erkut, and M. Karjalainen, "Blocked-based physical modeling for digital sound synthesis," *IEEE Signal Process. Mag.*, vol. 24, no. 2, pp. 42–54, Mar. 2007.
[31] F. Fontana and F. Avanzini, "Computation of delay-free nonlinear digital filter networks. Application to chaotic circuits and intracellular signal transduction," *IEEE Trans. Signal Process.*, vol. 56, no. 10, pp. 4703–4715, Oct. 2008.
[32] T. D. Rossing and N. H. Fletcher, *Principles of Vibration and Sound*. New York: Springer-Verlag, 1995.
[33] K. H. Hunt and F. R. E. Crossley, "Coefficient of restitution interpreted as damping in vibroimpact," *ASME J. Appl. Mech.*, vol. 42, pp. 440–445, Jun. 1975.
[34] H. M. Berger, "A new approach to the analysis of large deflections of plates," *ASME J. Appl. Mech.*, vol. 22, no. 4, pp. 465–472, 1955.
[35] R. Schmidt and D. A. DaPeppo, "A new approach to the analysis of shells, plates and membranes with finite deflections," *Int. J. Non-Linear Mech.*, vol. 9, no. 5, pp. 409–419, 1974.
[36] R. Jones, "A simplified approach to the large deflection of membranes," *Int. J. Non-Linear Mechan.*, vol. 9, no. 2, pp. 141–145, Apr. 1974.
[37] B. Bank, F. Avanzini, G. Borin, G. De Poli, F. Fontana, and D. Rocchesso, "Physically informed signal-processing methods for piano sound synthesis: A research overview," *EURASIP J. Appl. Signal Process.*, vol. 2003, no. 10, pp. 941–952, 2003.
[38] T. D. Rossing, I. Bork, H. Zhao, and D. O. Fystrom, "Acoustics of snare drums," *J. Acoust. Soc. Amer.*, vol. 92, no. 1, pp. 84–94, Jul. 1992.
[39] P. M. Morse, *Vibration and Sound*, 2nd ed. New York: McGraw-Hill, 1948.
[40] L. E. Kinsler, A. R. Frey, A. B. Coppens, and J. V. Sanders, *Fundamental of Acoustics*. Chichester, U.K.: Wiley, 2000.
[41] J. Obata and T. Tesima, "Experimental studies on the sound and vibration of drum," *J. Acoust. Soc. Amer.*, vol. 6, pp. 267–274, Apr. 1935.
[42] S. Bilbao, "Prepared piano sound synthesis," in *Proc. Int. Conf. Digital Audio Effects (DAFx-06)*, Montreal, QC, Canada, Sep. 2006, pp. 77–82.
[43] R. Marogna and F. Avanzini, "Physically based synthesis of nonlinear circular membranes," in *Proc. Int. Conf. Digital Audio Effects (DAFx-09)*, Como, Italy, Sep. 2009.

Federico Avanzini received the Laurea degree (*cum laude*) in physics from the University of Milano, Milan, Italy, in 1997 and the Ph.D. degree in information engineering from the University of Padova, Padova, Italy, in 2001 with a research project on sound and voice synthesis by physical modeling.

During the Ph.D. degree, he worked as a Visiting Researcher at the Laboratory of Acoustics and Audio Signal Processing, Helsinki University of Technology, Helsinki, Finland. Since 2002, he has been with the Sound and Music Computing Group, Department of Information Engineering, University of Padova, where he is currently an Assistant Professor, teaching courses in computer science and sound and music computing. His main research interests are in the area of sound synthesis and processing, with particular focus on musical sound synthesis, nonspeech sound in multimodal interfaces, and voice synthesis and analysis. He has been involved in numerous national and international (EU FP5, FP6) research projects, as well as industry-funded projects.

Riccardo Marogna received the Laurea degree in electronic engineering from the University of Padova, Padova, Italy, in 2005.

In 2006–2007, he received a scholarship from the University of Padova, within an EU-funded project. Since 2008 he has been a Research Fellow in the Department of Information Engineering of the same University. His main research interests concern algorithms for sound synthesis, multichannel sound processing, multimodal interfaces.